Composites: Part B 64 (2014) 97–107

Contents lists available at ScienceDirect

Composites: Part B

journal homepage: www.elsevier.com/locate/compositesb

Mechanical behaviour of corroded RC beams strengthened by NSM CFRP rods

Belal Almassri [a], Amjad Kreit [a], Firas Al Mahmoud [b], Raoul François [a,*]

[a] Université de Toulouse, UPS, INSA, LMDC (Laboratoire Matériaux et Durabilité des Constructions), France
[b] Institut Jean Lamour, UMR 7198, CNRS, Université de Lorraine, Nancy, France

ARTICLE INFO

Article history:
Received 21 January 2014
Received in revised form 14 March 2014
Accepted 20 April 2014
Available online 28 April 2014

Keywords:
A. Carbon fibre
B. Corrosion
B. Strength
D. Mechanical testing

ABSTRACT

Corrosion of steel in reinforced concrete leads to several major defects. Firstly, a reduction in the cross-sectional area of the reinforcement and in its ductility results in premature bar failure. Secondly, the expansion of the corrosion products causes concrete cracking and steel–concrete bond deterioration and also affects the bending stiffness of the reinforced concrete members, causing a reduction in the overall load-bearing capacity of the reinforced concrete beams. This paper investigates the validity of a repair technique using Near Surface Mounted (NSM) carbon-fibre-reinforced polymer (CFRP) rods to restore the mechanical performance of corrosion-damaged RC beams. In the NSM technique, the CFRP rods are placed inside pre-cut grooves and are bonded to the concrete with epoxy adhesive.

Experimental results were obtained on two beams: a corroded beam that had been exposed to natural corrosion for 25 years and a control beam, (both are 3 m long) repaired in bending only. Each beam was repaired with one 6-mm-diameter NSM CFRP rod. The beams were tested in a three-point bending test up to failure. Overall stiffness and crack maps were studied before and after the repair. Ultimate capacity, ductility and failure mode were also reviewed. Finally some comparisons were made between repaired and non-repaired beams in order to assess the effectiveness of the NSM technique. The experimental results showed that the NSM technique improved the overall characteristics (ultimate load capacity and stiffness) of the control and corroded beams and allowed sufficient ductility to be restored to the repaired corroded elements, thus restoring the safety margin, despite the non-classical mode of failure that occurred in the corroded beam, with the separation of the concrete cover due to corrosion products.

1. Introduction

Corrosion of reinforcing steel is still a very necessary area of study for infrastructure built of reinforced concrete. The cost of rehabilitating corroded RC structures world-wide exceeds $1.8 trillion per year [1]. The corrosion of steel bars in the RC elements is the underlying cause of many major defects. Firstly, it leads to a reduction in the cross sectional area of the steel reinforcement and a significant reduction in its ductility, which results in early failure of the steel bars. Secondly, the corrosion products increase the volume of the bars, setting up internal pressure that leads to the cracking of the RC elements and to bonding problems between the steel bars and the concrete. Corrosion also affects the bending stiffness of the RC elements [2–4]. The damage due to corrosion is difficult to evaluate and NDT methods do not permit the loss of cross-section to be determined. In contrast, destructive methods give information on the loss of cross-section but the results are largely scattered due to the heterogeneity of the corrosion pattern [5].

The consequences of corrosion on the residual mechanical properties of RC elements have been widely studied in recent decades. Experimental studies using electrically accelerated corrosion [6,7] or climate accelerated processes [8–10] have shown that the loss of load-bearing capacity is related to the maximum loss of cross-section: from 0.7% to 1.1% of loss in load-bearing capacity for 1% loss of cross-section. Corrosion of steel bars leads to a reduction in ultimate elongation [5,10,11], which induces a change in the failure mode of RC elements from classical ductile behaviour to brittle behaviour with a large reduction of ultimate deflection. For example, Khan et al. [8] recorded a total decrease of 53% in the ultimate deflection of a long-term corroded beam compared to a control beam, and a reduction of 17% in load bearing capacity when the cross-sectional loss in the corroded beam was 21.5%. Dang and François [9] found that the mechanical performance after 27 years of corrosion was reduced in terms of both ultimate load

* Corresponding author. Tel.: +33 561559901; fax: +33 561559900.
E-mail address: raoul.francois@insa-toulouse.fr (R. François).

http://dx.doi.org/10.1016/j.compositesb.2014.04.012
1359-8368/

capacity (26% loss of ultimate capacity in the corroded beam compared to the control beam) and ductility (47% loss of ductility in the corroded beam compared to the control beam). Thus, ductility can be expected to pose the major problem in respecting the rehabilitation standards for corroded RC members.

To increase the service life of corroded reinforced concrete structures, it is necessary to repair them and then to increase both their load bearing and deformation capacity. During recent years, many researchers have studied how to strengthen reinforced concrete elements using externally bonded fibre-reinforced polymer EBR (FRP) laminates [12–15]. A new strengthening technique called Near Surface Mounted (NSM) FRP reinforcement has attracted much research and practical applications. The NSM technique requires grooves to be cut in the concrete cover, in which the FRP reinforcement is then bonded to the concrete. Finally, the grooves are filled with epoxy or cement grout. Bilotta et al. [16] showed that the tensile strength of FRP material used in the NSM technique played a very beneficial role and that debonding was delayed compared to the EBR technique. The NSM FRP rods technique is considered to have some other advantages over other strengthening techniques such as EBR. De Lorenzis and Teng [17] note that the NSM bars are protected by the concrete cover and are thus less exposed to accidental damage like fire. They also point out that much less time and work is needed to fix and install the NSM FRP rods than externally bonded reinforcement (EBR).

In several cases, the strengthening of RC members by NSM CRFP rods can lead to non-conventional failure modes. For ordinary beams, the failure mode varies from rupture of the tensile reinforcement to compressive concrete crushing and it depends on the ratio between the tensile strength of the reinforcement and the compressive strength of the concrete. But, for strengthened RC members, the failure mode varies from degradation of the strengthening system to compressive concrete crushing and depends on the ratio of a combination of CFRP cross-section and CFRP length to the concrete compressive strength [18].

Ductility is an important structural design parameter in most design codes. In RC members, ductility is defined as the ratio of ultimate deformation to yield deformation and allows an indicator to be obtained that could be used for warning before failure. Previous studies have observed a ductility reduction in RC beams as a result of corrosion of the tensile steel bars [19,20].

Badawi and Soudki [21] showed a slight reduction in ductility for RC beams strengthened with NSM CFRP rods. Their results also showed that the ductility of the NSM CFRP strengthened beams was reduced as the prestressing level of RC beams increased. The NSM technique could have a small effect on the ultimate elongation of RC members when a classical failure mode is obtained [18]. On the other hand, it could lead to a more brittle and less ductile state in cases of non-classical failure such as peeling-off, which was observed by Al Mahmoud et al. [22], De Lorenzis et al. [23] and Radfar et al. [24], or pull-out of the CFRP rod, which was observed by Al Mahmoud et al. [25], De Lorenzis and Nanni [26] and De Lorenzis et al. [27].

The use of the NSM technique with FRP rods to repair and to strengthen infrastructure damaged by steel corrosion is very recent and few researchers have studied the subject. Kreit et al. [28] showed that the NSM technique allowed the initial ultimate capacity to be recovered for corroded beams with a 36% loss of cross-section in the maximum bending area. Ductile or brittle failure and the recovery of the ultimate elongation of corroded repaired RC members with NSM FRP rods have not yet been studied.

To improve understanding of the failure modes and the mechanical performance of repaired corroded beams, experimental work was undertaken to study the possibility of using a 6-mm-diameter NSM CFRP rod to repair a long-term naturally corroded RC beam and it was compared with a repaired control beam. The flexural capacity of the repaired beams was compared with that of non-repaired corroded beams. In a three point bending test, all beams were tested up to failure in order to study their overall bending moment-deflection behaviour, failure modes, stiffness properties and ultimate deflection. The corroded steel bars were extracted from the beams in order to study the corrosion and tensile tests were conducted to study the mechanical properties of the steel bars.

2. Experimental programme

An experimental programme was started at LMDC (Laboratory of Materials and Durability of Constructions in Toulouse, France) in 1984 with the aim of understanding the effects of steel corrosion on the structural behaviour of RC elements. This long-term programme consisted of casting a set of 72 RC beams of dimensions $3000 \times 280 \times 150$ mm. Thirty-six of them were stored in a chloride environment under service load to study the corrosion process. Many experimental studies have been performed on these beams to evaluate the development of corrosion cracking, measure the chloride content of the beams and analyse changes in their mechanical behaviour [19,29]. The other 36 beams were stored under the same mechanical load but in a non-aggressive environment to be used later as control beams in studies of long-term effects, such as creep and ageing of the concrete. The natural aggressive environment system consisted of a salt fog spray (35 g/l of NaCl) (see Fig. 1).

After 6 years of storage, the beams were subjected to wetting–drying cycles in order to accelerate the corrosion process:

- 0–6 years: continuous spraying under laboratory conditions ($T = 20$ °C).
- 6–9 years: cyclic spraying under laboratory conditions ($T = 20$ °C), 1 week of spraying and 1 week of drying.
- 9–19 years: cyclic spraying, 1 week of spraying and 1 week of drying, but the confined room was transferred outside, so the beams were exposed to monthly-average temperatures ranging from 5.1 °C to 21.3 °C.
- 19–27 years: cycles were stopped; the beams were still stored in the controlled room and exposed to the outside temperature.
- 27-present: cyclic spraying, 2 days of spraying and 12 days of drying.

The corrosion obtained in this climate-accelerated programme was very close to the corrosion observed under natural conditions in terms of corrosion distribution, corrosion type and oxides produced. It is very important for service life prediction of RC elements to have access to such natural degradation [30], rather than that

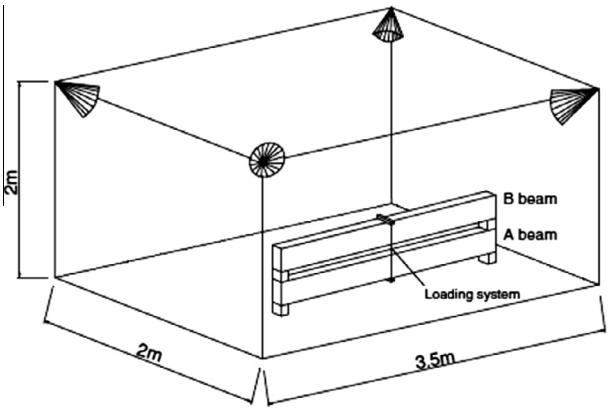

Fig. 1. The climate accelerated aggressive environment system.

resulting from the use of an applied current or a $CaCl_2$ admixture in the concrete [31,32]. The beams were divided into two groups named type A and type B, which had different reinforcement layouts but the same reinforcing steel bars (yield strength = 500 MPa). Beams A and B had 40 mm and 10 mm of concrete cover respectively. According to French standards at the time of manufacturing [33], 40 mm was the minimum concrete cover stipulated for very aggressive environments (i.e. chloride aggression) and the 10 mm was the minimum concrete cover in a non-aggressive environment. The beams were loaded in three-point flexure by coupling a type A beam with a type B beam. Two loading values were applied: M_{ser1} = 14 kN m for beams referred to as A1 (A1CL3-R and A1T-R) and M_{ser2} = 21 kN m for beams referred to as A2 (A2CL1, A2CL3, A2T and A2TI), which had the same type and shape of reinforcement but different values of service loading. The beams studied in this paper were type A beams; one corroded beam (A1CL3-R) and one control beam (A1T-R). Long-term corroded beams A2CL1, A2CL3, A2TI and A2T tested previously [8,9] but not repaired were also used here for comparison. The control beam A1T-R was strengthened using the same method as the one used to repair the corroded beam A1CL3-R. The layout of the reinforcement is shown in Fig. 2. For these beams, M_{ser1} represented the maximum loading value for durability in an aggressive environment for the type A beam (serviceability limit-state requirements in an aggressive environment).

2.1. Material properties

2.1.1. Concrete properties

The concrete mix is given in Table 1. The Water/Cement ratio was 0.5 but could be adjusted by changing the water quantity to obtain a constant workability of 7 cm in the slump test (slump class S2) in order to meet the most commonly specified consistence according to European Standard EN 206-1 [34]. The average compression stress and the elastic modulus obtained according to the standard on three cylindrical specimens (diameter 11 cm, height 22 cm) were 45 MPa and 32 GPa respectively at 28 days. The tensile strength, measured using the splitting test, was 4.7 MPa. Water porosity was 15.2%. To measure concrete characteristics, cylindrical cores, 70 mm × 140 mm, were drilled out of both the corroded and control beams and tested in compression. Table 2 gives the results of these core tests.

2.1.2. Characteristics of steel bars, CFRP bars and filling material

The steel reinforcing bars were composed of natural S500 half-hard steels; ordinary ribbed reinforcing steel bars were used. The steel bar characteristics were measured after extracting the corroded bars from the corroded beam A1CL3-R and the results are shown in Table 3

Al Mahmoud et al. [35] measured the mechanical properties of CFRP rods through a test programme conducted inn axial tension on 3 specimens. The CFRP rods showed brittle failure that started with splitting and ended with the failure of the rods as shown in Fig. 3. Table 4 shows the mechanical properties of the CFRP rods. In order to increase the bonding between the CFRP rods and the filling material, the rods were coated with 0.2/0.3 mm of surface sanding material which was sprinkled onto an epoxy paste applied to the surface of the rods.

Table 5 shows the characteristics of the filling material (epoxy paste) after 7 days [28].

Table 1
Concrete mix and cement chemical composition.

Mix component	mm	kg/m^3
Rolled gravel (silica + limestone)	5/15	1220
Sand	0/5	820
Portland cement: OPC HP		400
Water		200

Table 2
Mechanical characteristics of the concrete at 27 years (average of 3 tests).

Mechanical characteristics (MPa)	A1CL3-R	A1T-R
Compression strength	62.2	58.9
Elastic modulus	33,700	29,700

Table 3
Effective mechanical properties of steel bars (calculated from the residual cross-section).

Specimen number	Yield strength (MPa)	Avg	Ultimate strength (MPa)	Avg
Specimen 1 corroded	570	578	708	710
Specimen 2 corroded	585		711	
Specimen 1 non-corroded	595	600	640	645
Specimen 2 non-corroded	605		649	

2.2. Repair technique

The NSM CFRP rod was installed in the corroded beam A1CL3-R and in the control beam A1T-R by making two cuts in the concrete cover in the longitudinal direction on the tension side. A special concrete saw with a diamond blade was used.

The remaining concrete lug formed by the sawing was then removed using a hammer and hand chisel so that the lower surface became rough (Fig. 4). The groove was airbrushed to remove dust, debris and fine particles so as to ensure proper bonding between the paste and the concrete. Then, the groove was half filled and the CFRP rod was placed inside it and pressed lightly. This forced the paste to flow around the CFRP rod. More paste was applied to fill the groove and the surface was levelled. Thus, the CFRP rod was placed in the middle of the cross-section in the tension area.

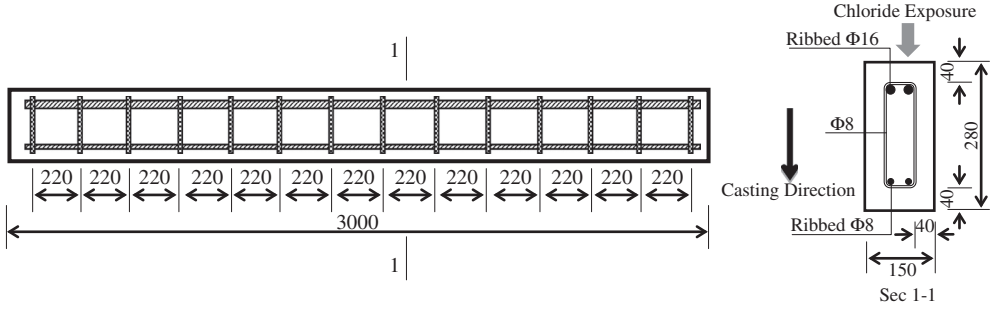

Fig. 2. Reinforcement layout for type A beams. Dimensions are in mm.

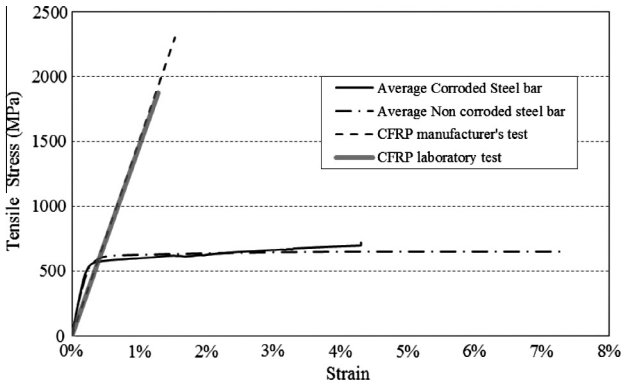

Fig. 3. Stress–strain diagrams for steel and CFRP bars.

Table 4
Characteristics of CFRP rods.

Type of test	Ultimate strength (MPa)	Modulus of elasticity (MPa)
Manufacturer's test	2300	150,000
Laboratory test	1875	145,900

Table 5
Filling material properties.

Material	Compressive strength (MPa)	Tensile strength (MPa)	Elastic modulus (MPa)
Epoxy	83	29.5	4900

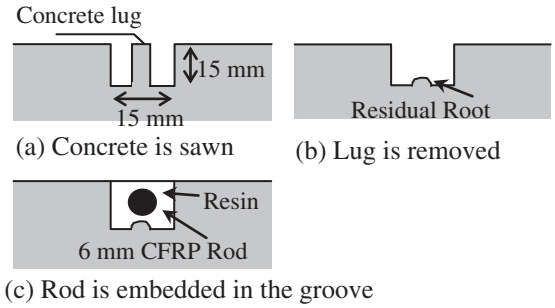

Fig. 4. Installation of CFRP rod into concrete surface.

The CFRP rod had a total length of 3000 mm and a diameter of 6 mm, which means that the repair was along the whole length of the beam. The groove was 15 mm deep and 15 mm wide (around twice the rod diameter). The two beams were tested 1 week after installation of the CFRP rod in order to ensure the maximum degree of adhesion between the concrete surface and the epoxy paste material.

2.3. Cracking maps of corroded beam A1CL3-R and control beam A1T-R

Figs. 5 and 6 show the cracking maps of the beams A1CL3-R and A1T-R after 26 years. All the corrosion cracks were concentrated in the tension area of the concrete and their maximum width was found to be 1.8 mm. Only the width of longitudinal cracks was measured using a binocular lens. The transversal cracks were due to the initial and sustained loading during beam storage. Despite the cover being the same for tension and compression bars, long-term storage in the chloride environment induced mainly corrosion and corrosion cracks along the tension reinforcement.

Dang and François [9] and Khan et al. [8] explained this result as a consequence of:

1. The difference in exposure between the tensile and compression faces; the tensile face was the upper horizontal face exposed directly to salt fog. 2. The casting direction: tension bars were also top bars according to the casting direction and exhibited some interface defects well known as top-bar effects. 3. The tensile face was cracked and the cracks in the upper surface exposed to chloride indicated the most aggressive environment (CEB-FIP model code).

3. Experimental results

3.1. Corrosion of steel bars

Clark's solution ANSI/ASTM G1-72 was used to remove the corrosion products from the surface of the steel bars, and then the diameter loss of the steel reinforcement bars due to corrosion was measured using two different methods. The first used a vernier calliper just after the steel bars had been cleaned and dried and the second used the weight loss of the steel bar to calculate the diameter loss. The second method required the critical parts of corroded steel bars to be cut into small pieces 1–2 cm long and then weighed to an accuracy of 0.001 g. A reference mass was measured on bars extracted from the control beam.

Both methods were used to evaluate the diameter loss of the corroded steel bars as some previous papers [5] had shown that the shape of corrosion damage was too complex to be measured only by the vernier calliper, which would give very conservative values of the diameter loss since the residual cross section varied considerably around the disk, as shown in Fig. 7.

3.2. Yielding moment and ultimate strength

Both the repaired corroded beam A1CL3-R and the repaired control beam A1T-R were tested using 3-point loading up to failure. Fig. 8 shows the bending moment vs. the deflection for the two beams. The yielding moment values for A1CL3-R and A1T-R were 41 kN m and 53 kN m, respectively, while the ultimate moment values were 52 kN m and 66 kN m respectively.

3.3. Failure modes

The classical failure of RC beams occurs either by concrete crushing or by the failure of the tensile steel bars. In the case of Type A beams, the failure of the control beam is normally due to steel bar yielding followed by concrete crushing [8]. After strengthening, the failure mode of RC beams can be concrete crushing, pull-out of the FRP rods or peeling off as shown by Al Mahmoud et al. [18]. The failure mode observed for A1CL3-R was different from both the conventional and non-conventional failure modes found on repaired non-corroded beams. The failure mode of the repaired corroded beam A1CL3-R was the separation of the concrete cover as shown in Fig. 9. The failure of the repaired control beam A1T-R occurred by the crushing of compressed concrete.

It should be noted that the failure plane corresponding to the separation of the concrete cover was the plane of corrosion cracks as shown in Fig. 10.

3.4. Losses of diameter due to corrosion for tensile steel bars and steel stirrups in corroded beam A1CL3-R

The values of the diameter losses were measured for both the Back Side (BS) and Front Side (FS) tensile steel bars, which were extracted from the corroded beam A1CL3-R just after the bending

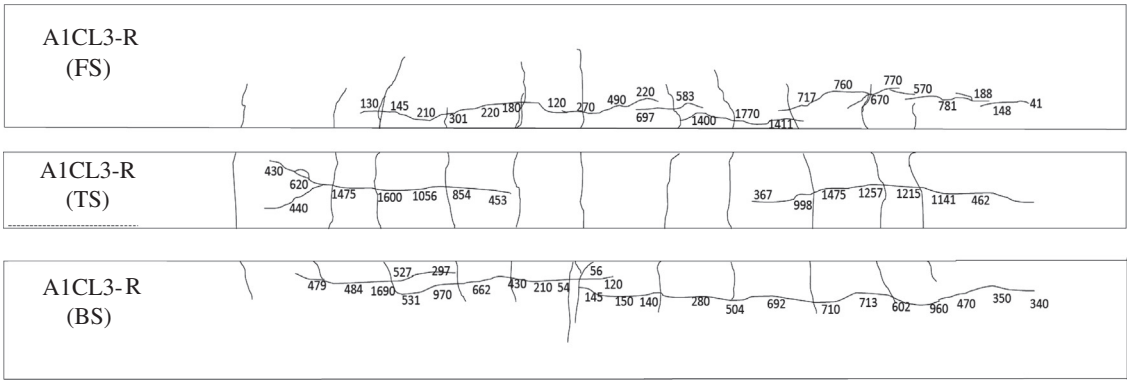

Fig. 5. A1CL3-R cracking map after 20 kN loading.

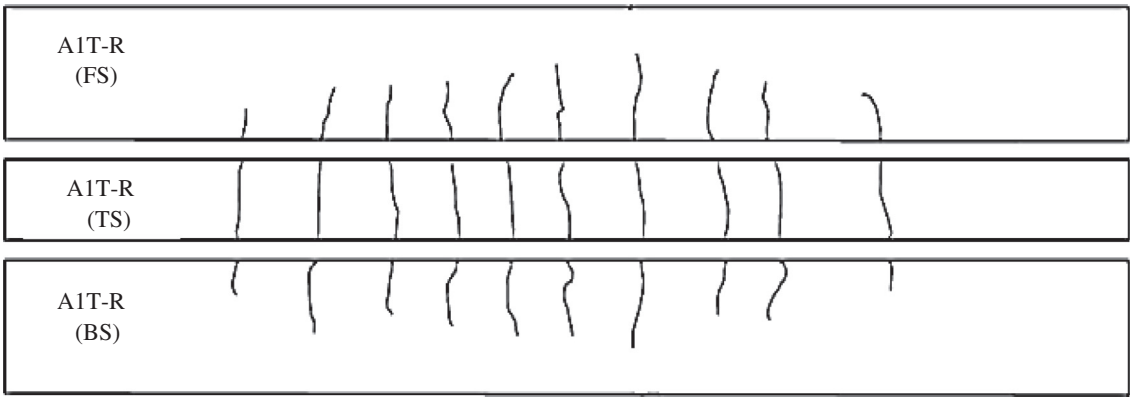

Fig. 6. A1T-R cracking map after 20 kN loading.

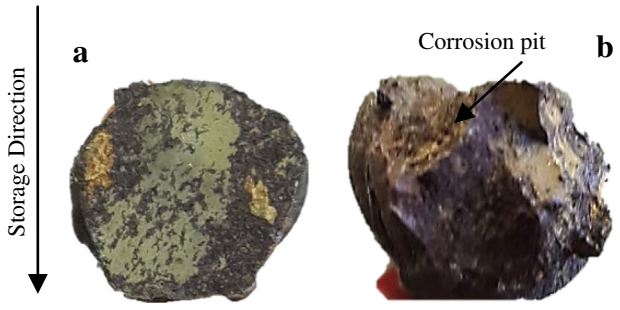

Fig. 7. Non-corroded bar (a) vs. corroded bar (corrosion pits) (b).

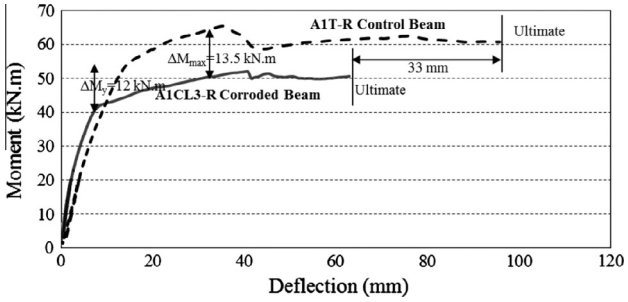

Fig. 8. Bending moment vs. deflection.

test. Figs. 11 and 12 show the diameter losses according to position along the whole length of the beam for BS and FS tensile steel bars. There is corrosion at the top of the bars close to the surface cover, which reflects the classical result for natural corrosion [31] and also at the bottom of the bars because of the effect of casting direction and bar location at the top of the beam, both of which induce poor interface quality [36,37].

The steel stirrups were numbered with respect to their parts (the first number represents the number of the part and the second number represents the number of the stirrup) as shown in Fig. 13.

Fig. 14 shows the locations of corrosion in the steel stirrups and the diameter values.

It can be seen from Fig. 14 that the stirrup corrosion map is in good agreement with the corrosion map for the longitudinal bars: parts of the stirrups in contact with compressive steel bars located at the bottom of the beam (according to casting direction) are not corroded, which agrees with the absence of corrosion in compressive longitudinal steel bars. On the other hand, parts of the stirrups in contact with tensile steel bars are corroded and, in some places, highly corroded, with 50% of cross-section loss. It should also be noted that there is no evidence of a difference in long-term corrosion damage of stirrups between those located near flexural cracks and those located in the non-cracked parts near the supports. This confirms that there is no relation between mechanical cracks and long-term natural corrosion as described by Beeby [38] and François et al. [39].

There was no corrosion along the vertical parts of stirrups located near the flexural cracks or even in the non-cracked area,

(a) A1CL3-R Corroded Beam (b) A1T-R Control Beam

Fig. 9. Beams after failure.

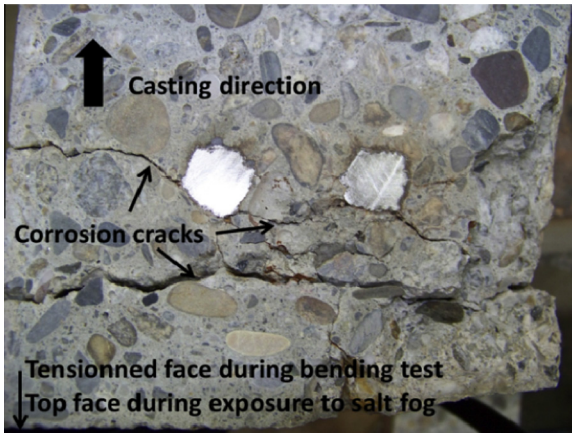

Fig. 10. Corrosion cracks appear in the concrete cover from the steel part closest to the tensile surface exposed to chloride.

which agrees with the long-term results presented by François et al. [39] and shows the beneficial effect of interface quality even in presence of cracks. The vertical surface here had a good interface quality and there was no mechanical damage or defects due to casting, such as bleeding.

3.4.1. Ultimate capacity

Table 6 and Fig. 15 present the ultimate bending moment capacity for repaired corroded and control beams, in comparison with non-repaired corroded and control beams. For non-repaired corroded beams, the residual ultimate load capacity is correlated with the maximum loss of cross-section: beam A2CL3, with 33% max. diameter loss in its tensile steel bars, shows a higher capacity than beam A2CL1 with 44% max. diameter loss in its tensile steel bars. The results also show that the repaired corroded beam

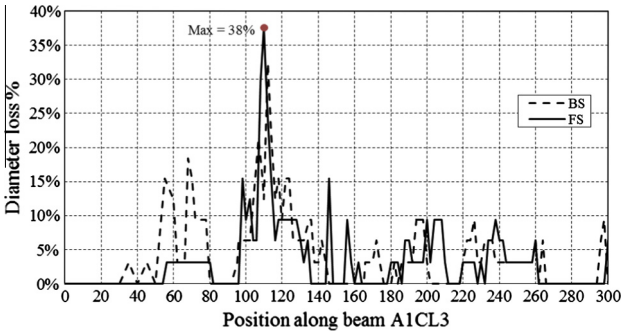

Fig. 12. Diameter loss percentages vs. position along the corroded beam A1CL3-R.

A1CL3-R (38% max. diameter loss in tensile steel bars) has a higher ultimate bending moment capacity than either A2CL1 or A2CL3 with17 kN m and 11 kN m respectively.

Fig. 15 also shows that both ultimate bending moment capacity and ultimate deflection of the control beam A1T-R (repaired using the NSM technique) ware higher than the ultimate capacity of non-repaired control beams A2T or A2TI.

3.4.2. Ultimate deflection

Fig. 16 presents the ultimate deflection values for corroded and control beams at failure points. The ultimate deflection value (93 mm) for repaired control beam A1T-R at the failure point was more than the ultimate deflection value for non-repaired control beams A2T (64 mm) and A2TI (64 mm). Results showed that the ultimate deflection value for repaired corroded beam A1CL3-R (63 mm) was higher than the ultimate deflection values for the corroded non-repaired beams A2CL3 and A2CL1 (28 mm and 30 mm respectively). On the other hand, the ultimate deflection for A1CL3 was almost the same as the ultimate deflection for non-repaired control beams A2T and A2TI. Thus, repairing the

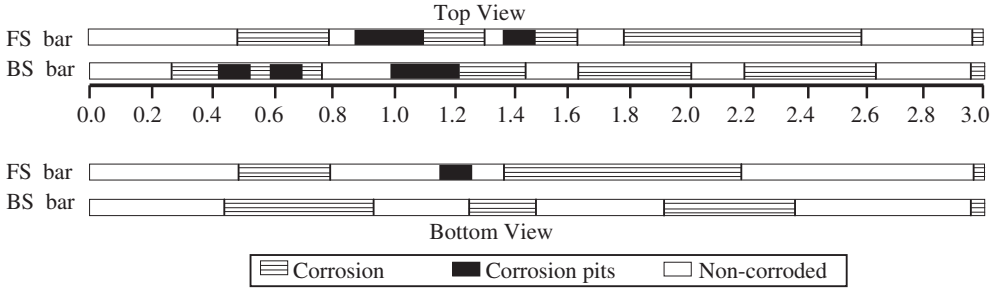

Fig. 11. Corrosion damage along re-bars according to the location in the beams (top or bottom).

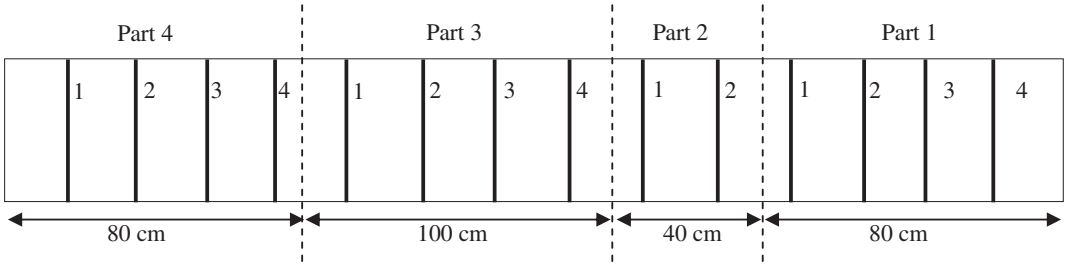

Fig. 13. Parts of beam A1CL3-R.

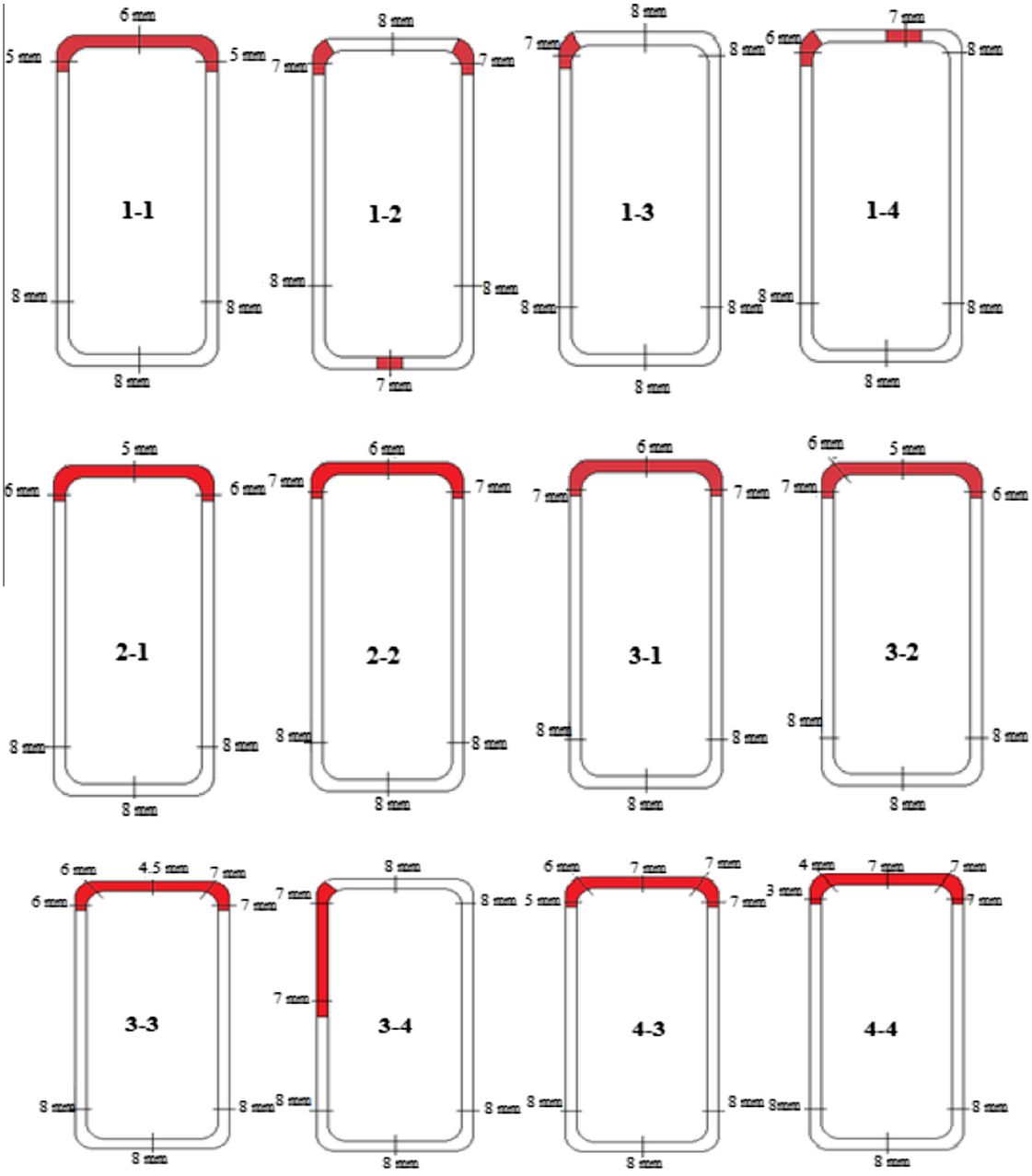

Fig. 14. Corrosion in steel stirrups of A1CL3-R.

corroded beam with the NSM technique doubles the ultimate deflection value compared to that of non-repaired corroded beams while the NSM repair increases the ultimate deflection for control beams 1.5 times relative to the non-repaired beams.

3.4.3. Percentage increase in the yielding capacity for beams repaired with NSM FRP rods

Fig. 17 presents the theoretical percentage increase in the repaired beams (shown in Appendix) over the non-repaired beams

Table 6
Experimental results for all beams.

Beam	Description	Max diameter loss % (1)	Failure mode	Ultimate moment (kN m)	Ultimate deflection (mm)	Ultimate Deflection loss % (2)	Ratio (2)/(1)
A1T-R	Repaired control beam	0	Concrete crushing	65.5	93	–	0
A1CL3-R	Repaired corroded beam	38	Separation of concrete cover	52.1	63	32[a]	0.84
A2T (Dang and François (9))	Non-repaired control beam	0	Concrete crushing	50.9	64	–	0
A2TI (Khan et al. (8))	Non-repaired control beam	0	Concrete crushing	49.7	63.8	–	0
A2CL3 (Khan et al. (8))	Non-repaired corroded beam	33	Failure of corroded steel bar	40.9	28	56[b]	1.7
A2CL1 (Dang and François (9))	Non-repaired corroded beam	44	Failure of corroded steel bar	35.6	29.9	53[b]	1.2

[a] Compared to repaired control beam A1T-R.
[b] Compared to non-repaired control beam A2T.

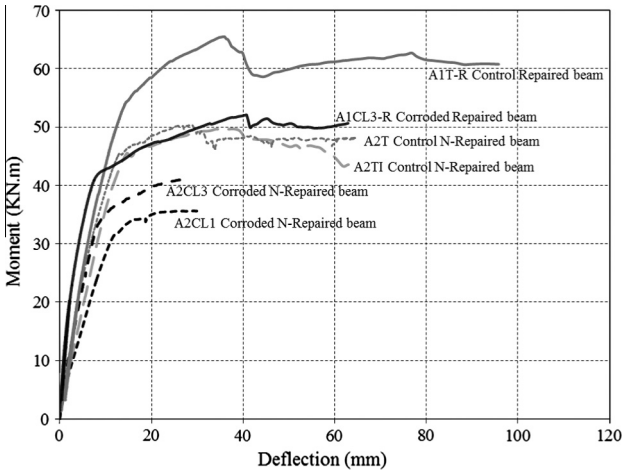

Fig. 15. Comparisons of moment capacity [A2T, A2TI, A1T-R, A2CL3, A1CL3-R and A2CL1 (8, 9)].

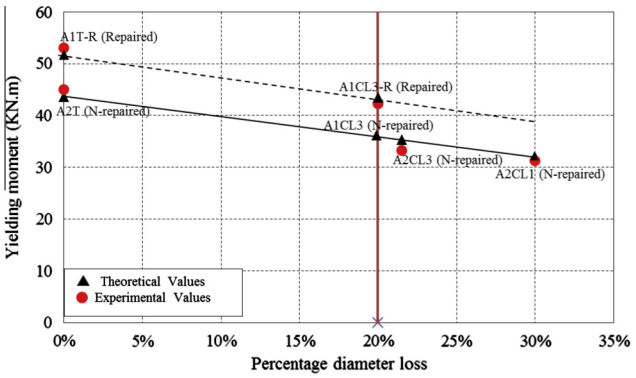

Fig. 17. Yielding capacity increase.

of type A in terms of yielding capacity in comparison with experimental results. An increase of 19% (Table 7) was recorded in the repaired corroded beam A1CL3-R compared to the non-repaired one while an increase of 18% was found in the repaired control beam A1T-R compared to A2T (non-repaired control beam tested by Khan et al. [8]). The percentage of difference between the repaired corroded beam A1CL3-R and the repaired control beam A1T-R was 20.7% due to the loss of steel diameter in the corroded beam (20%) assumed at the middle of the beam. Table 7 presents the details of the increase in yielding capacity for the beams A1CL3-R and A1T-R.

Fig. 17 also shows the percentage increase in My of the corroded (non-repaired) beams (A2CL3 and A2CL1). If they were repaired with the same process they would have shown increases

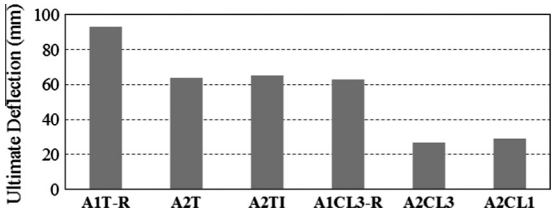

Fig. 16. Ultimate deflection (mm) for beams at failure.

Table 7
Calculated values of (yielding moment) My.

Beam	My, repaired (kN m)	My, non-repaired (kN m)	Percentage increase
A1CL3-R	43.5	36.5	19
A1T-R	51.7	43.7	18

of 18.9% and 18.8% respectively (almost the same increase for both beams as shown by the parallel lines in Fig. 17). This percentage increase falls as the percentage of steel diameter loss decreases.

3.4.4. Effect of corrosion on both yielding and ultimate capacity

Table 8 shows that every 1% loss of cross section corresponds to 1% loss of yielding capacity, while there is more scatter in the case of the ultimate capacity as the failure mode varies for each beam (e.g. 1% loss of cross section corresponds to 0.7% loss of ultimate capacity for A2CL3 while it corresponds to 1.1% for A2CL1 and 1% for A1CL3-R).

3.4.5. Stiffness of beams

The two beams A1CL3-R and A1T-R were loaded with a 20 kN service load before starting the repair process. They were also tested with 20 kN after the repair with NSM. Fig. 18 shows the values of the stiffness (the slope value before the yielding point is reached) for both beams before and after the repair process (stiffness ratio).

Table 8
Comparison of loss of cross sections against the loss of ultimate capacity and yielding capacity experimental values.

Beam	Avg loss of cross section % at the middle (1)	Yielding capacity (kN m)	Ultimate capacity (kN m)	Loss of yielding capacity % (2)	Loss of ultimate capacity % (3)	(3)/(1) ratio	(2)/(1) ratio
A2T	0	45	50.9	0	0	0	0
A2CL3	21.5	32.5	40.9	27.8	19.6	0.7	1
A2CL1	30	31.3	35.6	30.4	34	1.1	1
A1T-R	0	53	65.5	0	0	0	0
A1CL3-R	20[a]	42.3	52.1	20.6	20.5	1	1

[a] *Note:* My = 42.3 kN m occurs with 20% loss of cross section at the middle of the beam.

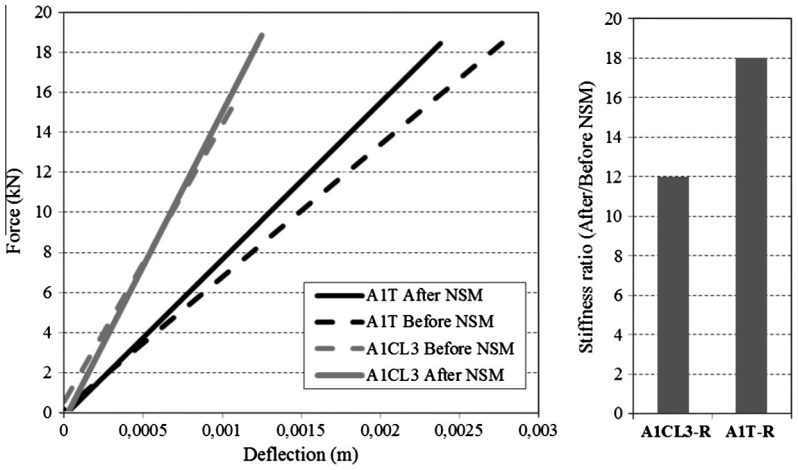

Fig. 18. Stiffness ratio for repaired beams.

Table 9
Ductility index values.

Beam	Ultimate deflection value (Δu) mm	Yielding deflection value (Δy) mm	Ductility index
A1T-R	93	15	6.2
A1CL3-R	63	9	7.0
A2T	64	14.5	4.4
A2TI	63.8	14.5	4.4
A2CL1	29.9	12.5	2.4
A2CL3	28	11.2	2.5

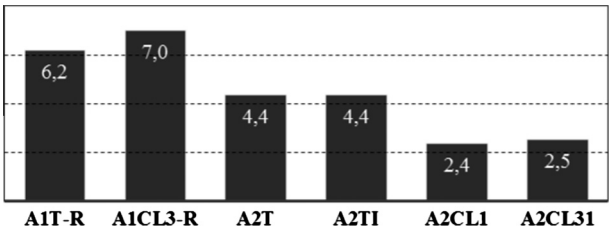

Fig. 19. Ductility index chart.

The stiffness of cracked beams depends on the number of cracks and the crack spacing, and could be affected by the degree of corrosion. The repair process using 6-mm-diameter rods increased the stiffness of the two beams (A1CL3-R and A1T-R) before the yielding point with almost the same ratio: 12% and 18% respectively.

3.4.6. Ductility

Ductility is the ability of the structures to sustain large deformations without a decrease in load resistance and it is necessary for RC beams to provide early warning of failure. Ductility has generally been measured by a ratio called the ductility factor or index ($\Delta u/\Delta y$) corresponding to a deformation (such as curvature, deflection, rotation) at failure (Δu) divided by the corresponding value at yielding (Δy) (Classical definition by Badawi and Soudki [21]). Ductility index values were calculated and are presented in Table 9 and Fig. 19.

The ductility of corroded beams decreases 5 times for each 1% loss of cross section but this could be unacceptable for the safety of a corroded structure. The NSM technique allows the initial ductility of the beam before corrosion to be recovered as shown in Fig. 19.

3.4.7. Failure modes

The failure mode observed on repaired corroded beam A1CL3-R was different from those on non-repaired corroded beams A2CL1 and A2CL3, which failed by brittle failure of the tension steel bar at deep corrosion pits. Failure of repaired corroded beam A1CL3-R occurred by a non-conventional mode due to the existence of a rupture plane induced by corrosion cracks. This plane was parallel to the concrete tensile surface but located at steel bar level so it was easy to remove the concrete cover from the reinforcing skeleton. This failure mode was observed by Kreit et al. [28] for a corroded beam of type B with 1 cm of concrete cover repaired with a 6-mm NSM CFRP rod. On the other hand, the failure mode of repaired control beam A1T-R was classical: yielding of the steel bars occured, followed by crushing of the compressive concrete. The use of transversal strengthening could be an option to avoid the specific failure mode of separation of concrete cover (or spalling) induced by corrosion of the tensile reinforcement.

4. Conclusions

According to the experimental results found in this paper, the following conclusions can be drawn:

1. The NSM technique is able to increase the ultimate load capacity of a corroded beam that has suffered considerable damage and can allow it to reach to the ultimate capacity of the control beam.
2. The efficiency of the NSM technique in repairing corroded beams could be limited by the separation of the concrete cover due to corrosion induced cracks.
3. The NSM technique slightly increases the stiffness of both repaired corroded and repaired control beams.
4. The NSM technique increases the ultimate deflection value for repaired control and corroded beams.
5. The NSM technique restores sufficient ductility (2.8 times that of the non-repaired corroded beams) after ductility loss due to the brittle behaviour of corroded RC beams because of steel corrosion.
6. If there is 1% cross-section loss due to steel corrosion it will be reflected as a 1% loss in the yielding capacity value. The percentage is different for ultimate capacity as the mode of failure is not the same in each case: 1% increase due to NSM corresponds to 1% (dc/ds) increase in yielding moment.
7. Because of its efficiency, the NSM technique could be a promising way to repair RC structures damaged by corrosion. Nevertheless, the appearance of a new non-conventional failure mode needs more investigation to propose a relevant method of design that provides safe design margins.

Appendix A. Classical RC calculations

Table 10 presents the values calculated for the moment of the corroded beam A1CL3-R and the control beam A1T-R based on the classical mode of failure for RC beams by concrete crushing (Equations used in Al Mahmoud et al. [18] as shown in figure 20, with *b*: width of beam; ds: effective depth of beam; h: height of beam; fy: yielding stress of steel bars; Es: modulus of elasticity of steel bars; Ef: modulus of elasticity of FRP bars; As: cross sectional area of steel bars; Af: cross sectional area of FRP bars.

The values used for the calculations were, for A1CL3-R: b = 15 cm, h = 28 cm, ds = 22.4 cm, Es = 200 GPa, Ef = 150 GPa, As = 3.42 cm^2, Af = 0.28 cm^2, fy = 578 MPa and, for A1T-R: b = 15 cm, h = 28 cm, ds = 22.4 cm, Es = 214 GPa, Ef = 150 GPa, As = 4.02 cm^2, Af = 0.28 cm^2, fy = 600 MPa. As mentioned before, the high degree of corrosion and the increase in shear stresses in the concrete cover prevented the beam from reaching the maximum theoretical value of the classical failure mode and it failed by the separation of the concrete cover. More studies need to be conducted on this new mode of failure in order to understand its mechanism.

Table 10
Summary of calculated values of moment.

Beam	Yielding bending moment My (kN m)		Ultimate bending moment My (kN m)	
	Calculated	Experimental	Calculated	Experimental
A1CL3-R	43.5	42.3	63.4	52.1
A1T-R	51.7	53	68.4	65.5

References

[1] Schmitt G. Global needs for knowledge dissemination, research, and development in materials deterioration and corrosion control. NY: World Corros Organ; 2009.
[2] Al-Sulaimani G, Kaleemullah M, Basunbul I, Rasheeduzzafar. Influence of corrosion and cracking on bond behaviour and strength of reinforced concrete members. ACI Struct J 1990;87(2):220–31 (ASTM G1. 1990).
[3] Andrade C, Alonso C, Garcia D, Rodriguez J. Remaining lifetime of reinforced concrete structures: effect of corrosion on the mechanical properties of the steel. 1991.
[4] Cairns J, Plizzari GA, Du Y, Law DW, Franzoni C. Mechanical properties of corrosion-damaged reinforcement. ACI Mater J 2005;102(4).
[5] François R, Khan I, Dang VH. Impact of corrosion on mechanical properties of steel embedded in 27-year-old corroded reinforced concrete beams. Mater Struct 2013;46(6):899–910.
[6] Torres-Acosta AA, Navarro-Gutierrez S, Terán-Guillén J. Residual flexure capacity of corroded reinforced concrete beams. Eng Struct 2007;29(6):1145–52.
[7] Malumbela G, Moyo P, Alexander M. A step towards standardising accelerated corrosion tests on laboratory reinforced concrete specimens. J South Afr Inst Civ Eng 2012;54(2):78–85.
[8] Khan I, François R, Castel A. Structural performance of a 26-year-old corroded reinforced concrete beam. Eur J Environ Civ Eng 2012;16(3–4):440–9.
[9] Dang VH, François R. Influence of long-term corrosion in chloride environment on mechanical behaviour of RC beam. Eng Struct 2013;48:558–68.
[10] Zhu W, François R. Corrosion of the reinforcement and its influence on the residual structural performance of a 26-year-old corroded RC beam. Constr Build Mater 2014;51:461–72.
[11] Almusallam AA. Effect of degree of corrosion on the properties of reinforcing steel bars. Constr Build Mater 2001;15(8):361–8.
[12] Sherwood E, Soudki K. Confinement of corrosion cracking in reinforced concrete beams using carbon fiber reinforced polymer laminates. ACI Spec Publ 1999:188.
[13] Soudki KA, Sherwood TG. Behaviour of reinforced concrete beams strengthened with carbon fibre reinforced polymer laminates subjected to corrosion damage. Can J Civ Eng 2000;27(5):1005–10.
[14] Steiner W. Strengthening of structures with CFRP strips. Montreal, Quebec, Canada: Canadian Society for Civil Engineers; 1996. p. 407–19.
[15] Soudki K. FRP Repair of Corrosion-damaged Concrete Beams — Waterloo Experience. In: Pandey M, Xie W-C, Xu L, editors. Advances in engineering structures, mechanics & construction [Internet]. Netherlands: Springer; 2006. p. 165–73. http://dx.doi.org/10.1007/1-4020-4891-2_14.
[16] Bilotta A, Ceroni F, Di Ludovico M, Nigro E, Pecce M, Manfredi G. Bond efficiency of EBR and NSM FRP systems for strengthening concrete members. J Compos Constr 2011;15(5):757–72.

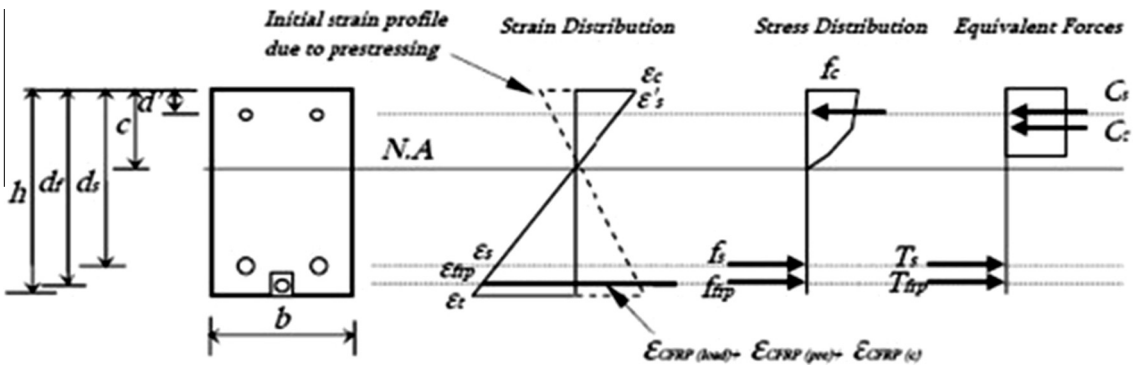

Fig. 20. Forces equilibrium and strain distribution for RC beams.

[17] De Lorenzis L, Teng J. Near-surface mounted FRP reinforcement: an emerging technique for strengthening structures. Compos Part B Eng 2007;38(2):119–43.
[18] Al-Mahmoud F, Castel A, François R, Tourneur C. Strengthening of RC members with near-surface mounted CFRP rods. Compos Struct 2009;91(2):138–47.
[19] Castel A, François R, Arliguie G. Mechanical behaviour of corroded reinforced concrete beams—Part 1: experimental study of corroded beams. Mater Struct 2000;33(9):539–44.
[20] Du Y, Clark LA, Chan AH. Impact of reinforcement corrosion on ductile behavior of reinforced concrete beams. ACI Struct J 2007;104(3).
[21] Badawi M, Soudki K. Flexural strengthening of RC beams with prestressed NSM CFRP rods–experimental and analytical investigation. Constr Build Mater 2009;23(10):3292–300.
[22] Al-Mahmoud F, Castel A, François R, Tourneur C. RC beams strengthened with NSM CFRP rods and modeling of peeling-off failure. Compos Struct 2010;92(8):1920–30.
[23] De Lorenzis L, Micelli F, La Tegola A. Passive and active near surface mounted FRP rods for flexural strengthening of RC beams. 2002.
[24] Radfar S, Foret G, Saeedi N, Sab K. Simulation of concrete cover separation failure in FRP plated RC beams. Constr Build Mater 2012;37:791–800.
[25] Al-Mahmoud F, Castel A, François R. Failure modes and failure mechanisms of RC members strengthened by NSM CFRP composites–Analysis of pull-out failure mode. Compos Part B Eng 2012;43(4):1893–901.
[26] De Lorenzis L, Nanni A. Bond between near-surface mounted fiber-reinforced polymer rods and concrete in structural strengthening. ACI Struct J 2002;99(2).
[27] De Lorenzis L, Nanni A, La Tegola A. Flexural and shear strengthening of reinforced concrete structures with near surface mounted FRP rods 2000:521–8.
[28] Kreit A, Al-Mahmoud F, Castel A, François R. Repairing corroded RC beam with near-surface mounted CFRP rods. Mater Struct 2011;44(7):1205–17.
[29] Vidal T, Castel A, François R. Corrosion process and structural performance of a 17 year old reinforced concrete beam stored in chloride environment. Cem Concr Res 2007;37(11):1551–61.
[30] Poursaee A, Hansson C. Potential pitfalls in assessing chloride-induced corrosion of steel in concrete. Cem Concr Res 2009;39(5):391–400.
[31] Yuan Y, Ji Y, Shah SP. Comparison of two accelerated corrosion techniques for concrete structures. ACI Struct J 2007;104(3).
[32] Otieno M, Beushausen H, Alexander M. Prediction of corrosion rate in reinforced concrete structures–a critical review and preliminary results. Mater Corros 2012;63(9):777–90.
[33] French regulations for reinforced concrete structures. B.A.E.L. 1983.
[34] EN 206-1. European standard, concrete – Part 1: specifications, performance, production and conformity. NF EN 206-1; April. 2004.
[35] Al-Mahmoud F, Castel A, François R, Tourneur C. Effect of surface pre-conditioning on bond of carbon fibre reinforced polymer rods to concrete. Cem Concr Compos 2007;29(9):677–89.
[36] Horne A, Richardson I, Brydson R. Quantitative analysis of the microstructure of interfaces in steel reinforced concrete. Cem Concr Res 2007;37(12):1613–23.
[37] Soylev T, François R. Quality of steel–concrete interface and corrosion of reinforcing steel. Cem Concr Res 2003;33(9):1407–15.
[38] Beeby A. Concrete in the oceans: cracking and corrosion. Cem Concr Assoc 1978.
[39] François R, Castel A, Vidal T, Vu N-A. Long term corrosion behavior of reinforced concrete structures in chloride environment. J Phys IV Fr 2006 Nov;136:285–93.